Analyst

PAPER

View Article Online
View Journal

Cite this: DOI: 10.1039/d5an00518c

A ratiometric green-to-blue emitting Hg^{2+} ion-responsive ionic liquid-based micro-optode†

Shubham Lama, Sabbir Ahamed, Shraddha Rai, Upika Darnal, Subekchha Pradhan, Najmin Tohora and Sudhir Kumar Das *

Received 11th May 2025,
Accepted 30th June 2025

DOI: 10.1039/d5an00518c

rsc.li/analyst

This study presents an Hg^{2+} ion-responsive ratiometric green-to-blue emitting ionic liquid (IL), trihexyltetradecylphosphonium hydroxyproline-1,3,6-trisulfonate (**HPTIL**), and its micro-optode, **mHPTIL**. Neat **HPTIL** functioned as a photoluminescent ink without a solvent, highlighting its effectiveness as a safe-keeping script material and served as a green-to-blue-emitting Hg^{2+} ion-responsive photoluminescent IL. Upon the introduction of heavy metal Hg^{2+} ions into the water-suspended **mHPTIL** system, a noticeable ratiometric shift from greenish to bluish fluorescence was observed, exhibiting detection and quantification limits in the nanomolar (nM) range with the lowest LOD of 1.67 nM. Additionally, a very convenient and portable solid-state paper-strip-based test kit was introduced to monitor the heavy metal, Hg^{2+} ions. This work proposes a novel approach for generating low-dimensional materials based on ILs that have exceptional properties for environmental and forensic monitoring.

Introduction

Mercury is one of the most hazardous and non-biodegradable heavy metals, posing serious threats to the human health and environment. Paints, batteries, and electronic equipment are just a few of the frequent industrial and domestic products that release mercury into the environment.[1–3] As industries continue to expand, the potential risk of exposure to hazardous heavy metal ions also increases.[4–7] Mercury is a hazardous heavy metal found in many natural sources on the Earth and is produced *via* weathering, combustion, and volcanic activity. Studies have shown that since industrialization began, mercury levels in the environment have tripled. Approximately half of the mercury released because of human activities originates from coal combustion for energy production. Mercury can spread widely from its source and become a worldwide threat in its elemental state as it remains in the atmosphere for a long period. Mercury-contaminated drinking water can lead to various health issues, including decreased kidney function, abnormalities in the development of the baby's brain, and harm to the development of fetus in pregnant women.[8,9] Mercury pollutants can transform into methylmercury when absorbed by smaller organisms and plants, which is a highly potent and well-known neurotoxin for the human body.[9–11] This toxic compound then accumulates in the human body as it moves up the food chain. However, mercury pollutants can also enter the body through the skin, respiratory system, and digestive tract, leading to serious kidney and stomach disorders owing to their strong affinity for thiol groups in proteins and enzymes.[12–14] The U.S. Environmental Protection Agency (EPA) classifies mercury as a highly hazardous element and limits mercury ion concentration in drinking water to 10 nM.[15] Although many countries have taken steps to clean the environment and lower industrial emissions, global mercury pollution remains a serious threat to the human health.[16] In Japan, infants and unborn children are particularly vulnerable to seafood poisoning caused by elevated mercury levels.[17]

Hg(II) in both organic and inorganic compounds can readily cross biological membranes and cause severe harm to organisms, even at low concentrations.[10,18,19] The most common form of Hg(II) compounds is $HgCl_2$, from which the detection of Hg(II) is both practical and significant. However, $HgCl_2$ is a covalent compound that primarily exists in a molecular state, with only a small fraction dissociating into $HgCl^+$ and Cl^- in aqueous solutions. Hg^{2+} is also rare in $HgCl_2$ aqueous solutions.[20] If $HgCl_2$ undergoes ionization into Hg(II) ions, such as $HgCl^+$ and Hg^{2+}, it can be identified using heavy metal ion (HMI) fluorescent sensors.

Conventional techniques used for mercury ion detection include electrochemical analysis,[21,22] atomic absorption spectrometry,[23] atomic emission spectrometry, inductively coupled plasma-mass spectrometry,[24] surface-enhanced Raman spectroscopy,[25,26] anodic stripping voltammetry,[27] and atomic fluorescence spectrometry.[28] These techniques, however, require costly equipment and labor-intensive, time-consuming

Department of Chemistry, University of North Bengal, Raja Rammohunpur, Darjeeling, West Bengal-734013, India.. E-mail: sudhirkumardas@nbu.ac.in

† Electronic supplementary information (ESI) available. See DOI: https://doi.org/10.1039/d5an00518c

processes that are suitable only for highly qualified professionals. Conversely, colorimetric or fluorometric detection has drawn interest as a viable method for detecting Hg^{2+} ions because of its ease of use, affordability, high selectivity, and real-time monitoring capabilities. Consequently, fluorescent optodes have garnered significant attention owing to their advantages, including high selectivity, ease of use, no need for pretreatment, and suitability for on-site detection, making them one of the simplest and most accessible chemosensing methods compared to other available detection techniques. Recently, Tohora *et al.* developed a pyrene butyrate-based IL-derived crystalline nanoball that causes blue fluorescence quenching owing to the addition of Hg^{2+} ions.[29] Sultana *et al.* developed a 'turn-on' fluorogenic probe that selectively detects Hg^{2+} ions.[30] Ali *et al.* designed an optical chemosensor film that selectively detects Hg^{2+} ions.[31] Hu and Yu *et al.* successfully developed a rhodamine-based sensor that displays high selectivity towards Hg^{2+} ions.[32] Subsequently, Wang *et al.* designed and synthesized a new peptide-based fluorescent chemosensor for selective detection of Hg^{2+} ions.[33]

For almost 2 decades, ionic liquids (ILs), which are organic salts with a melting point usually lower than 100 °C (lower than those of ionic salts such as sodium chloride (NaCl) owing to the presence of two sterically incompatible ions disrupting the packing of the crystal lattice[34–36]) have been the subject of intense chemical research. The wide variety of uses of ILs is the reason for this continued interest. The earliest examples of ILs can be linked to Walden, who aimed to create a molten salt that remains liquid at room temperature, as well as Atwood's research on "red oil".[37,38] Over the past few decades, interest in this field has grown significantly, turning it into a major research "drift".[37] ILs are one of the few chemical compounds that have developed so quickly.[39] Green solvents,[40] electrolytes,[41,42] lubricants,[43,44] liquid crystals,[40] white-light generation,[45] heat storage fluids,[46,47] separation and extraction stages,[48,49] soft materials,[50–52] catalysts,[53–55] metal sensors and biocatalysis[56] are some chemistry applications for these organic salts. Furthermore, the industrial sector has become more interested in ILs, as evidenced by the integration of ILs as solvents into industrial processes.[36] Certain ILs remain in a liquid state at room temperature (25 °C) and are referred to as room-temperature ILs, while others are solid at 25 °C but melt below 100 °C, known as frozen ILs. Warner and his team introduced a novel class of organic salts, naming them a "group of uniform materials based on organic salts" (GUMBOS).[57,58] GUMBOS have melting points ranging from 25 °C to 250 °C. Nanoparticles, known as nano-GUMBOS, can be synthesized from these materials using a straightforward reprecipitation method by adjusting the length of their aliphatic side chains. These nano-GUMBOS hold promising applications in sensing, energy conversion, and the biomedical field.[59–64]

In recent years, ILs have focused on various fields. Finally, ILs as chemosensors have a great advantage, with numerous reports of a developing chemo-fluorosensor. Moreover, ILs have been added to enhance the intensity of fluorescence in some systems. ILs promote a new technique for emerging functional optoelectronic materials by integrating advantageous physicochemical characteristics into their fundamental structure, which outperforms conventional ones, making them suitable for detecting target analytes. Many studies have reported the use of ILs as chemosensors for target analytes, such as ILs for the on-site monitoring of trace gaseous SO_2,[62] re-useable IL-based colorimetric organo nanosensors for the detection of nerve agent stimulants,[63] IL-based ratio fluorescent sensors for real-time visual monitoring of trace Hg^{2+},[65] and rhodamine-based ILs for the ultra-sensitive and selective detection of mercury ions.[66]

Given the numerous advantages of ILs, we propose the development of an organo-nanosensor utilizing an IL-based micro-optode by incorporating a pyranine derivative. This sensor is designed for the selective and highly accurate detection of heavy metal ions, specifically Hg^{2+}. We synthesized an IL containing a pyranine trisulfonate anion through a straightforward ion exchange process involving the sodium salt of pyranine trisulfonate and trihexyltetradecylphosphonium chloride ($P_{66614}Cl$). From this IL **HPTIL**, we thoroughly examined the photophysical characteristics of their pure form and further applied them as photoluminescent security inks for writing applications. Their aggregation behavior has been extensively investigated using spectro-microscopic techniques. Notably, aqueous-suspended microparticles, **mHPTIL**, which emit bright green fluorescence when exposed to a UV lamp of 365 nm, have been effectively employed as fluorescent sensors for detecting Hg^{2+} ions. These IL-based nano-optodes display high selectivity, outstanding stability, on-site detection, and precise quantification abilities.

Experimental section

Using the method established by Baker and colleagues,[67] our optode **HPTIL** was synthesized. The data for this study, including the synthetic procedure for **HPTIL**, fabrication of **mHPTIL**, materials, equipment, and experimental techniques, are provided in the ESI.†

Results and discussion

Characterization of HPTIL and mHPTIL

The characterization of the synthesized **HPTIL** was confirmed using various traditional analytical methods. The results of the ^1H NMR study validate **HPTIL**'s fruitful synthesis (Fig. S1†). Additionally, the analysis of liquid chromatography–mass spectrometry (LCMS) demonstrates that the m/z peak at 483.3934 is associated with the cationic phosphonium component. Conversely, the signal at m/z 469.1149 infers $[HPTS]^{3-}$ anion presence combined with atomic nitrogen, as shown in Fig. S2,†[68] indicating that during the electrospray ionization process, a nitrogen adduct is formed. Two distinctive stretches were visible in the spectrum of Fourier transform infrared spectroscopy (FT-IR) at 2962 and 2924 cm^{-1}, corresponding to

asymmetric stretching vibrations, along with two additional bands at 2882 and 2856 cm^{-1} ascribed to symmetric stretching vibrations, respectively. These conclusions further support the effective formation of **HPTIL** (Fig. S3†). **HPTIL** gives the impression of a viscous fluid at ambient temperature, suggesting that the synthesized organic salt establishes IL-like properties.

In contrast to **HPTIL** in DMSO solution, the spectra of UV-visible absorption of **mHPTIL** show a noticeably wide band with a bathochromic shift of around 4 nm, as displayed in Fig. 1a, inferring that the HPTS moiety forms J-type aggregation within the core of the ILs. Hence, to validate the J-type aggregation formation of HPTS in the water-suspended **mHPTIL**, we performed **HPTIL**'s aggregation behavior with different DMSO–water fractions. Specifically, when the water fraction was high, we observed a redshift in the UV-visible absorption spectra in the presence of Mie scattering. These spectral characteristics indicate the formation of J-type aggregation (Fig. S5a and b†) of the HPTS moiety within IL-derived water-suspended microparticles. The **HPTIL** solution of 100% water–DMSO resulted in a maximum redshift of 4 nm with a peak having maxima at 404 nm. The emission characteristics of the free **HPTIL** probe were also studied across different water percentages (Fig. S5c†). Our observations indicate that an increase in water percentage corresponded to a decrease in fluorescence intensity, implying that aggregation causes quenching (ACQ). The maximal photoluminescence intensity of **HPTIL** was recorded at 416 nm in a 0% water–DMSO solution (Fig. S5c†). The establishment of HPTS's J-type aggregation inside the core IL-based low-dimensional materials is confirmed by the observation of a redshift of the UV-visible absorption spectra and the notable Mie-scattering seen from the water suspension, as shown in (Fig. 1a). According to a λ^{-4} dependency, Rayleigh-type scattering is responsible for the prolonged tail at longer wavelengths in the aqueous suspension's absorption spectrum.[69] High-resolution dynamic light scattering (DLS) measurements, as shown in Fig. 1c, and scanning electron microscopy (SEM) analysis, as displayed in Fig. 1b, provide additional confirmation of the existence of low-dimensional structures of water-suspended **mHPTIL**. Analysis of the SEM images confirms the hydrodynamic radius of 1729.9 ± 10 nm found in the DLS spectrum. The effective formation of **mHPTIL** is shown by the rod-shaped morphology of the **mHPTIL** microparticles dissolved in water. An extensive network of H-bonds between HPTS and water molecules results in low-dimensional materials with rod-like shapes. The observed zeta potential (ζ) of the microparticle in an aqueous medium is 37 ± 10 mV, as shown in Fig. S4.† A high ζ indicates a large positive surface charge, and in water, the microparticle improves its firmness. Furthermore, the hydrophobic core of the microparticles encapsulates the HPTS's negatively charged part, which successfully keeps them inside the structure.[70] To assess its long-term performance, we subjected **mHPTIL** to continuous UV light exposure and monitored its photoluminescence at several time intervals. The results, presented in Fig. S6,† confirm that **mHPTIL** exhibits robust photostability, demonstrating its suitability for applications requiring resilience to UV light over time.

Spectroscopy behaviour of neat HPTIL

When excited at 330 nm, our synthesized neat **HPTIL** displays a robust emission peak at 439 nm. Remarkably, the emission bands did not show any mirror images of the excitation band of one another (Fig. 2a). Pure **HPTIL** demonstrates cyanish photoluminescence, equivalent to a CIE coordinate of x = 0.147, y = 0.100, as shown in Fig. 2b. This distinctive spectroscopic behavior indicates that **HPTIL** has potential as a next-generation fluorescent ink. Photoluminescent ink pens globally aim at security applications, and the versatility of ILs in using various printing methods, including 3D and fine printing, may broaden the future potential of **HPTIL**-based inks. At present, IL-based ink pens rank among the most widely used writing gadgets worldwide. In this study, **HPTIL** was tested as a prototypical ink under neat environments using Whatman filter paper 41. **HPTIL** was successfully embedded into a microtip, and the letters "NBU" were framed to evaluate it. The neat **HPTIL**'s appearance is illustrated, which occurs under both normal and UV light (Fig. 3a–d). Surprisingly, when exposed to a 365 nm UV laser, the framed letters show high brilliance and intense cyanish photoluminescence. The letters must maintain excellent photostability for real-world applications, such as information encryption and anti-counterfeiting, under different environmental circumstances. As a consequence of the hydrophobic nature of neat **HPTIL**, under watery

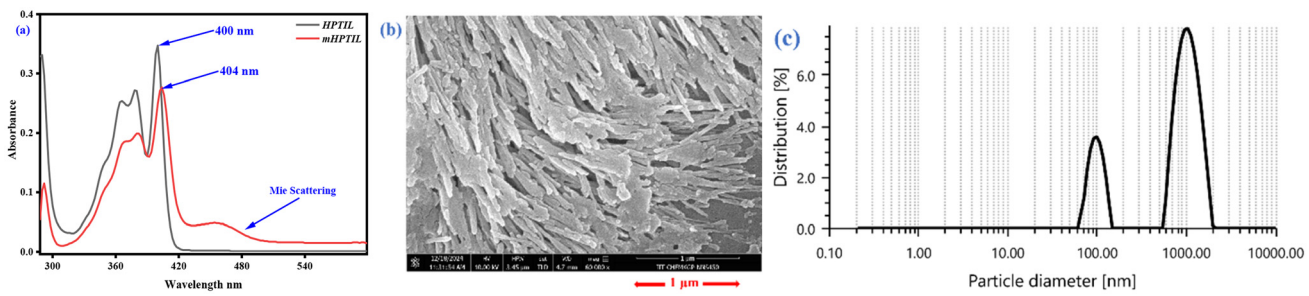

Fig. 1 (a) UV-vis absorption spectra of **HPTIL** (29 µM) and **mHPTIL** (29 µM). (b) Scanning electron microscopy image of **mHPTIL**. (c) Dynamic light scattering spectrum of **mHPTIL**.

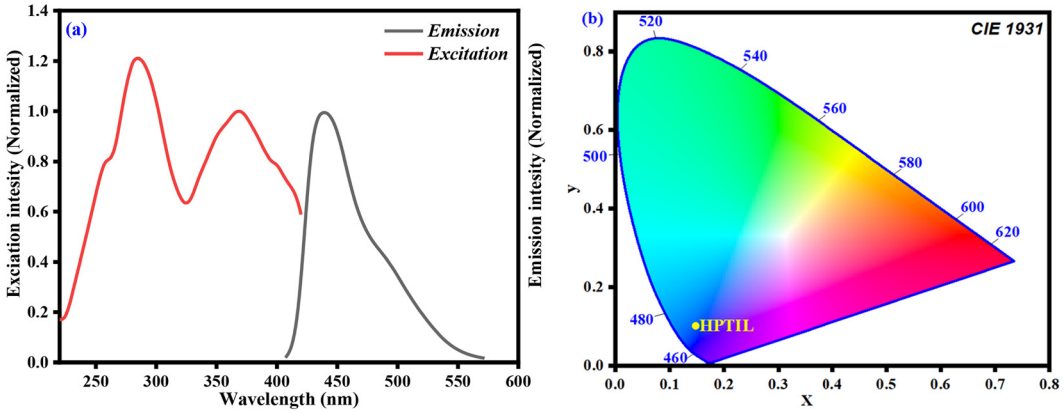

Fig. 2 (a) Excitation and emission spectra of pure HPTIL and (b) conformation to the CIE illustration (x = 0.147, y = 0.100).

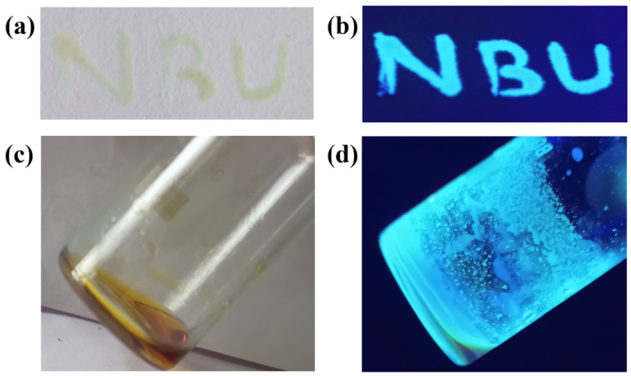

Fig. 3 (a) and (b) Letters "NBU" framed on Whatman filter paper 41, as observed under visible light and UV lamp exposure, respectively. (c) and (d) Images of pure HPTIL captured in natural daylight and under 365 nm UV lamp irradiation.

conditions, the letters hold up nicely. The superior optical stability of IL-based photoluminescent inks, such as **HPTIL**, paves the way for their broader application across various fields.

Spectroscopic response of mHPTIL towards various metal ions

We examined the characteristics of fabricated **mHPTIL** microparticles using UV-visible absorption spectroscopy. The UV-visible absorption spectra showed a noticeable shift in the absorption peak when water-soluble Hg^{2+} was added. In particular, a 4 nm blue shift was noted after the addition of Hg^{2+}, and the peak wavelength changed from 404 nm to 400 nm, as displayed in Fig. 4a.

Currently, fluorosensors are at the forefront of heavy metal detection because of their high sensitivity, clear signal output, portability, fast response time (within a few seconds), and user-friendly operation. In line with this approach, we investigated the fluorescence behavior of our designed micro-optode using fluorometric titration experiments. Considering the advantages of the fluorometric technique, we conducted fluorescence-based investigations to evaluate the sensing performance of our **mHPTIL** for detecting heavy metal, Hg^{2+}. To accomplish this, photoluminescence titration spectra of water-suspended **mHPTIL** are obtained with various other metal chlorides. For water-dispersible microparticles, **mHPTIL** shows an emission peak at 515 nm, and with the gradual addition of Hg^{2+} (0–96 μM), the peak at 515 nm gradually decreased while simultaneously generating a new peak at 426 nm, as shown in (Fig. 4b), changing the fluorescence color from green to blue. The UV-visible absorption spectral results and fluorometric observations suggest that the SO_3^- group present in **HPTIL** interacts with heavy metal Hg^{2+}, resulting in a blue shift in the UV-visible absorption and photoluminescence spectra. As illustrated in Scheme 1, the interaction of Hg^{2+} with the SO_3^- group of our optode removes the $[P_{66614}]^+$ ions from the core of **mHPTIL**. Further, Hg^{2+} is well-coordinated with the hydroxyl (–OH) functional group of HPTS, which participates in the water-mediated excited state intermolecular proton transfer process within the core of **mHPTIL**. Since our optode bears $3SO_3^-$ and one –OH functional group, four Hg^{2+} ions bind successively with the one unit of HPTS present in the **mHPTIL**, demonstrating a 1 : 4 (HPTS : Hg^{2+}) stoichiometric ratio, which is further confirmed from the job plot[71] analysis, as shown in (Fig. 5d). Owing to the well-coordination of $3SO_3^-$ and one –OH functional groups involved in the HPTS moiety with Hg^{2+} ions, the water-mediated excited state intermolecular proton transfer process is inhibited owing to the coordination of Hg^{2+} ions. Consequently, the emission peak at 515 nm gradually decreased with the simultaneous generation of a new peak located at 426 nm, changing the fluorogenic color from green to blue with a distinct isoemissive point at 477 nm, which is also confirmed by the CIE diagram analysis; this shows a distinct change in coordinate values from (x = 0.170, y = 0.614) that is under the color gamut of green fluorogenicity to (x = 0.160, y = 0.129) belongs to blue photoluminosity, as displayed in (Fig. 4c). The ratiometric plot of $[Hg^{2+}]$ *versus* the intensity ratio (I_{426}/I_{515}) demonstrates a robust linear relationship, as shown in (Fig. 4d), highlighting the optode's capability for the precise quantification of unknown Hg^{2+} concentrations with minimal error. In contrast, similar concentrations of various

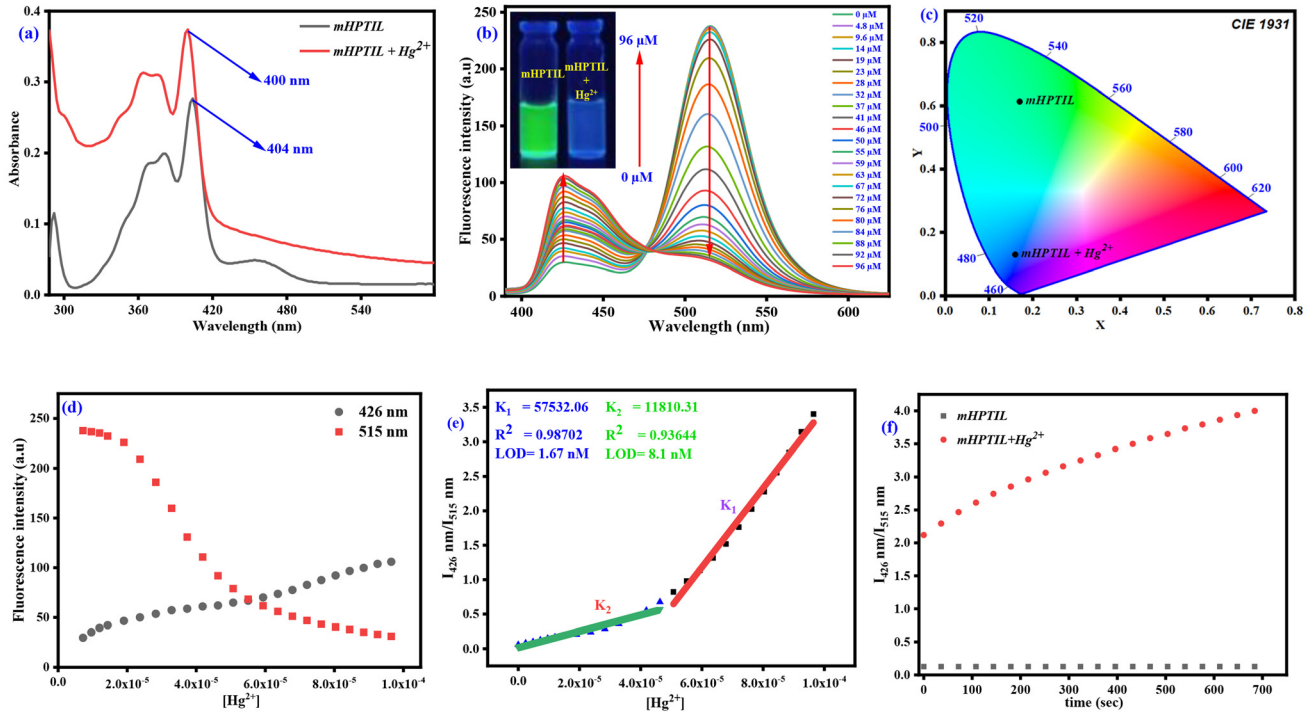

Fig. 4 (a) UV-visible absorption spectra of **mHPTIL** (29 μM) and **mHPTIL** (29 μM) with the addition of Hg^{2+} (50 μM). (b) Monitoring photoluminescence intensity of **mHPTIL** (29 μM) in aqueous solution with a gradual increase in Hg^{2+} (0–96 μM), λ_{exc} at 330 nm. (c) CIE diagram illustrating the change in color gamut for **mHPTIL** (29 μM) against **mHPTIL**-Hg^{2+} (96 μM). (d) Deviation in the photoluminescence spectra of **mHPTIL** (29 μM) upon the addition of Hg^{2+} (96 μM) at 426 nm and 515 nm. (e) Detection limit between the emission intensity ratio (I_{426}/I_{515}) and Hg^{2+} concentrations in the range of 0–41 μM and 50–96 μM. (f) Deviation in the photoluminescence band correlation (I_{426}/I_{515}) of **mHPTIL** (29 μM) against **mHPTIL**-Hg^{2+} (96 μM) with time.

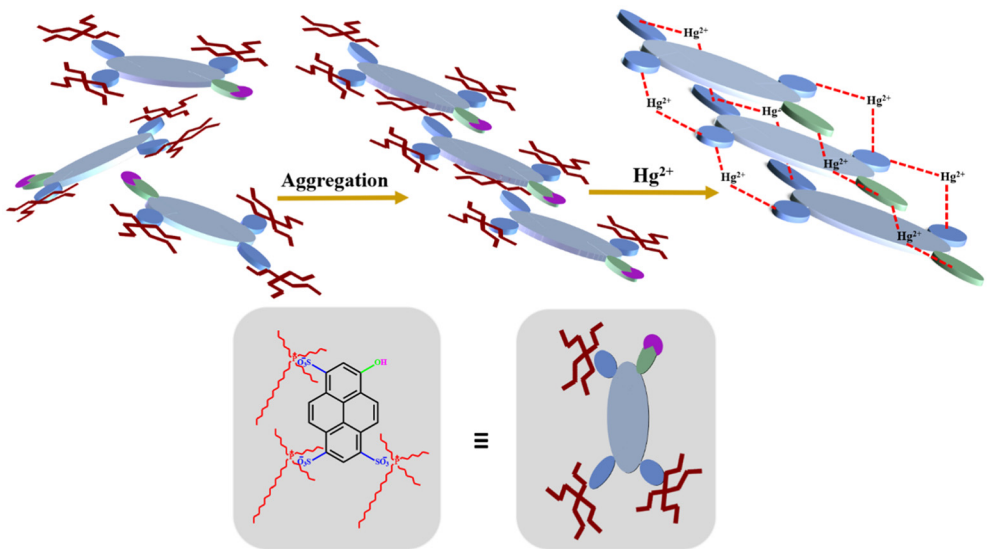

Scheme 1 Mechanistic pathway of the interaction of Hg^{2+} ions with **mHPTIL**.

other metal chlorides did not cause any significant fluorescence changes. The Benesi–Hildebrand (B–H) equation[72] $\frac{1}{F-F_{min}} = \frac{1}{K(F-F_{min})[Hg^{2+}]} + \frac{1}{F_{max}-F_{min}}$ was used to calculate the binding constant for the interaction between **mHPTIL** and Hg^{2+}. The ratio of the intercept to the slope of the resulting linear plot was used to compute the binding constant, represented by '*K*'. The **mHPTIL** optode's minimal emission intensity at 426 nm is denoted by 'F_{min}' in this analysis, the emission intensity at 426 nm for different Hg^{2+} concentrations

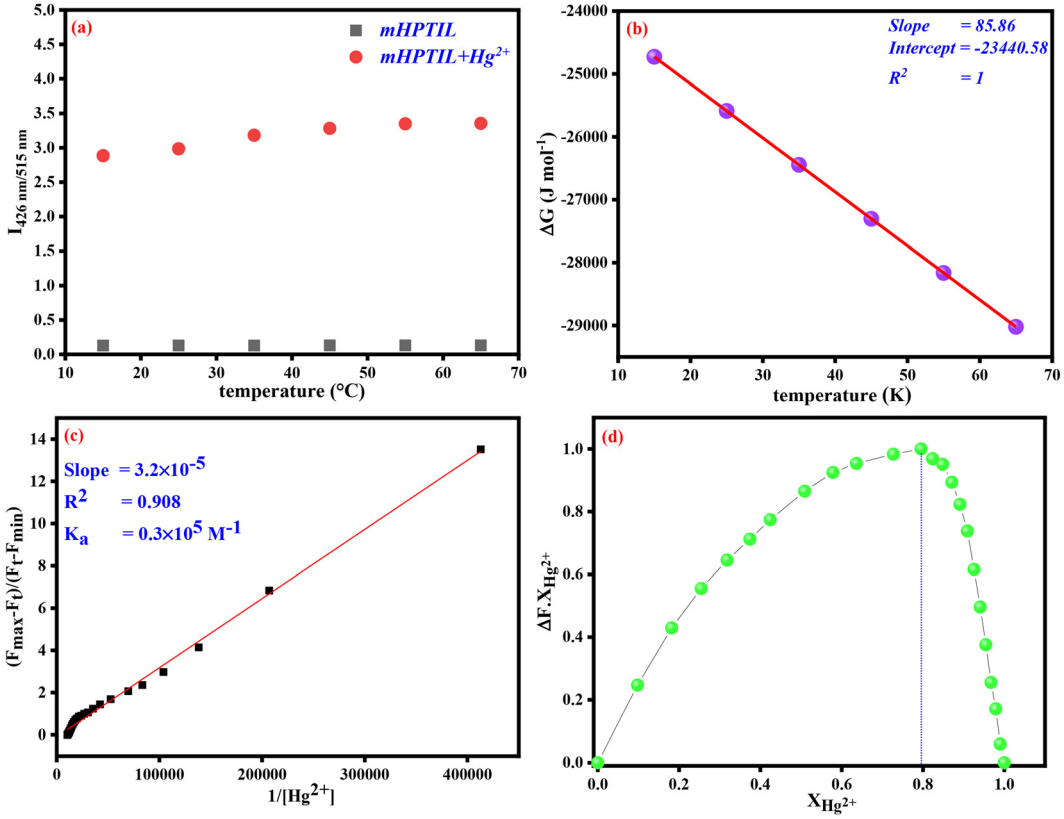

Fig. 5 (a) Temperature-dependent fluorescence study of **mHPTIL** and **mHPTIL**-Hg^{2+} complex. (b) Linear calibration curve for calculating the ΔH and ΔS values. (c) Benesi–Hildebrand plot of **mHPTIL**-Hg^{2+} complex, demonstrating the binding affinity towards Hg^{2+}. (d) Job's plot in the **mHPTIL** : Hg^{2+} ratio of 1 : 4.

by F, and the maximum emission intensity recorded during Hg^{2+} titration by 'F_{max}'. [Hg^{2+}] indicates the Hg^{2+} concentration used during fluorometric titration. Using this approach, the **mHPTIL**–Hg complex's binding constant with Hg^{2+} ions was found to be 0.3×10^5 M^{-1} (Fig. 5c).

Important factors affecting a chemosensor's capacity to identify and quantify target analytes at low concentrations are the detection limit (LOD) and quantitation limit (LOQ). Using eqn (1) and (2),

$$\mathrm{LOD} = \frac{3\sigma}{K}, \quad (1)$$

$$\mathrm{LOQ} = \frac{10\sigma}{K}, \quad (2)$$

we estimated the values following the IUPAC recommendations. Here, 'σ' denotes the standard deviation, which was determined from 10 repeated emission intensity measurements of **mHPTIL** without Hg^{2+}, and 'K' denotes the slope of the calibration curve, which was obtained from the plot of (I_{426}/I_{515}) *versus* Hg^{2+} concentrations, where we obtained two slopes K_1 = 57 532 over the range of 50–96 μM and K_2 = 11 810.31 over the range 0–41 μM, respectively, with linear regression coefficients values R_1^2 = 0.98 and R_2^2 = 0.93, respectively. The resulting plot demonstrates two significant linear associations over the concentration range of (0–41 μM) and (50–96 μM). These findings showed that **mHPTIL** works better for Hg^{2+} detection than several previously published fluorescence sensors, with LOD ranging from 1.67 nM to 8.1 nM, which falls within the tolerance border range established by the WHO and EPA (30 nm and 10 nm, respectively).[73] (Table S1†) LOQ values are obtained ranging from 5.56 nM to 27 nM, respectively, as demonstrated in (Fig. 4e). The present results demonstrate that **mHPTIL** could be an effective ratiometric fluorescence chemosensor based on IL that can detect Hg^{2+} ions with high sensitivity. The van't Hoff equations[74,75] are

$$\ln(K_a) = -\frac{\Delta H}{RT} + \frac{\Delta S}{R} \quad (3)$$

$$\Delta G = \Delta H - T\Delta S \quad (4)$$

where R denotes the universal gas constant, T represents the absolute temperature, ΔH denotes the change in enthalpy, ΔS denotes the change in entropy and ΔG denotes the change in Gibbs free energy at varying temperatures. We plotted a linear calibration curve between ΔG and T using the Van't Hoff equation (Fig. 5b). The values of ΔH and ΔS are found from the slope and intercept of the corresponding plot, respectively. As shown in (Table S1†), ΔH is found to be negative, signifying

that the interaction between Hg^{2+} and **mHPTIL** is exothermic. Additionally, (Table S1†) reveals a positive value for ΔS, suggesting an increase in system entropy during the interaction. Previous studies[76] have suggested that such a thermodynamic pattern of negative enthalpy and positive entropy can be attributed to electrostatic interactions. Hence, the opposite charges of **mHPTIL** and Hg^{2+} support the conclusion that the formation of the hybrid system is primarily governed by electrostatic forces. Furthermore, the negative ΔG value (as shown in Table S1†) confirms that the interaction between **mHPTIL** and Hg^{2+} occurs spontaneously.

Analysis of response time and kinetics

The superiority of chemosensors, such as quick response, simple visual detection under UV light and with the unaided eye, and affordable measurements, has attracted a lot of attention, in which response time plays a crucial role. A time-dependent fluorometric response in the case of the detection of heavy metals, such as Hg^{2+}, with our optode, **mHPTIL**, was investigated through fluorometric analysis. The study included monitoring how the **mHPTIL** photoluminescence intensity changed over time when Hg^{2+} was introduced. To monitor the progress of these alterations, photoluminescence spectra were recorded at predetermined intervals of 0–6 minutes. The intensity peak at 426 nm was observed to increase, whereas the original peak at 515 nm immediately decreased. The interaction between **mHPTIL** and Hg^{2+} is further supported by the apparent change in photoluminescence from green to blue. Both qualitative and quantitative information about the sensor's response was provided by the observed visual change, which matched the spectral data. By timing the site concerning photoluminescence intensity correlating between 426 nm and 515 nm stabilized at their greatest value, the response time of **mHPTIL** for detecting Hg^{2+} was evaluated. The results established the **mHPTIL** optode's quick response to Hg^{2+}, with noticeable spectrum alterations emerging a few seconds after Hg^{2+} was introduced, as demonstrated in Fig. 4, underscoring the sensor's quick response capabilities. Additionally, we investigated the kinetics of our complex using the equation $\ln\frac{F_{max}-F_t}{F_{max}} = -kt$. The conclusion suggests that the reaction proceeds *via* pseudo-first-order kinetics towards the Hg^{2+} ion, which is 0.003 s^{-1}, with constant (k) and F_t denoting photoluminescence at F_{426}/F_{515} at the given time 't' (Fig. S7†).

Photoluminescence response of mHPTIL to various ions

Selectivity and sensitivity are crucial parameters in the development of chemosensors for sensing applications. To evaluate the selectivity of the synthesized water-suspended microparticles, **mHPTIL** (29 μM), fluorescence titration experiments were conducted in the presence of various water-soluble metal chlorides, such as Al^{3+}, Ba^{2+}, Ca^{2+}, Cd^{2+}, Co^{2+}, Cu^{2+}, Zn^{2+}, Fe^{3+}, Hg^{2+}, Mg^{2+}, Mn^{2+}, Ni^{2+}, Pb^{2+}, and Fe^{2+}. When 96 μM of different metal ions were added, there were no discernible changes in our **mHPTIL** solution's absorption spectra, except for the observation of significant Mie scattering in the case of Hg^{2+} ions. However, there was a discernible change from green to blue in the photoluminescence spectroscopy when Hg^{2+} ions were present. Additionally, the photoluminescence response of **mHPTIL** with 96 μM Hg^{2+} compared to different metal ions is illustrated in (Fig. 6a). Interestingly, the optode exhibits strong selectivity for Hg^{2+} ions when irradiated under a 365 nm UV lamp with no significant photoluminescence shift observed when the other metal ions are added to the solution of **mHPTIL**, as shown in (Fig. 7a). Under similar conditions, various water-soluble anions, such as $Al(PO_4)$, K_2CO_3, KBr, KCl, NaF, $NaBH_4$, Na_2HPO_4, NaH_2PO_4, Na_3PO_4, KPF_6, Na_2S and Na_2SO_4, were conducted. Fascinatingly, no such significant photoluminescence change was observed in comparison to Hg^{2+}, as displayed in (Fig. 6b), indicating a high selectivity of our synthesized water-suspended microparticles, **mHPTIL**, towards the Hg^{2+} within various potent water-soluble metals and non-metals.

It is essential for the selective detection of Hg^{2+} ions in the presence of competing cations because metal ions, such as Fe^{3+}, Cu^{2+}, Cd^{2+}, Pb^{2+}, Zn^{2+}, Mg^{2+}, and Ni^{2+}, often coexist with Hg^{2+} in a range of environmental water sources. We conducted a comprehensive interference investigation in this respect by contrasting the photoluminescence spectra of the water-suspended **mHPTIL** complex in the presence of Hg^{2+} ions. Interestingly, the presence of other competing metal ions does not affect the fluorescence spectra of the **mHPTIL**-Hg^{2+} complex, as shown in (Fig. 6c). This suggests that even when various interfering cations are present, the **mHPTIL** optode maintains remarkable selectivity towards Hg^{2+} ions, underscoring its possible use in environmental sample analysis. Additionally, we examined the emission response of **mHPTIL** (29 μM) in the presence of multiple water-soluble anions, including $AlPO_4$, K_2CO_3, KBr, KCl, NaF, $NaBH_4$, Na_2HPO4, NaH_2PO_4, Na_3PO_4, KPF_6, Na_2S, and Na_2SO_4, as illustrated in Fig. 6d. The results demonstrated that these anions did not affect the fluorescence intensity of the **mHPTIL**-Hg^{2+} complex, indicating that **mHPTIL** can selectively detect Hg^{2+} ions even in complex ionic environments. Based on the aforementioned results, it may be inferred that the water-suspended **mHPTIL** optode has the potential to be used in environmental sample analysis because it can selectively detect Hg^{2+} ions in complex ionic gathering environments.

Effect of pH on sensing

To assess **mHPTIL**'s potential for detecting Hg^{2+} ions under physiological conditions, it is important to understand how pH influences its sensory response. Our approach includes preparing a series of HEPES buffer solutions with distinct pH values achieved by carefully titrating with HCl and NaOH. Afterward, photoluminescence tests are carried out in each of these buffer solutions. The results of these tests are crucial in determining **mHPTIL**'s suitability for Hg^{2+} ion detection in biological environments. As shown in Fig. S8,† the fluorescence intensity ($I_{426\ nm/515\ nm}$) of **mHPTIL** was very weak across the pH range of 5–12. The fluorescence intensity ($I_{426\ nm/515\ nm}$) changes noticeably with the addition of Hg^{2+} ions, with the emission intensity being maximum at pH 7.22.

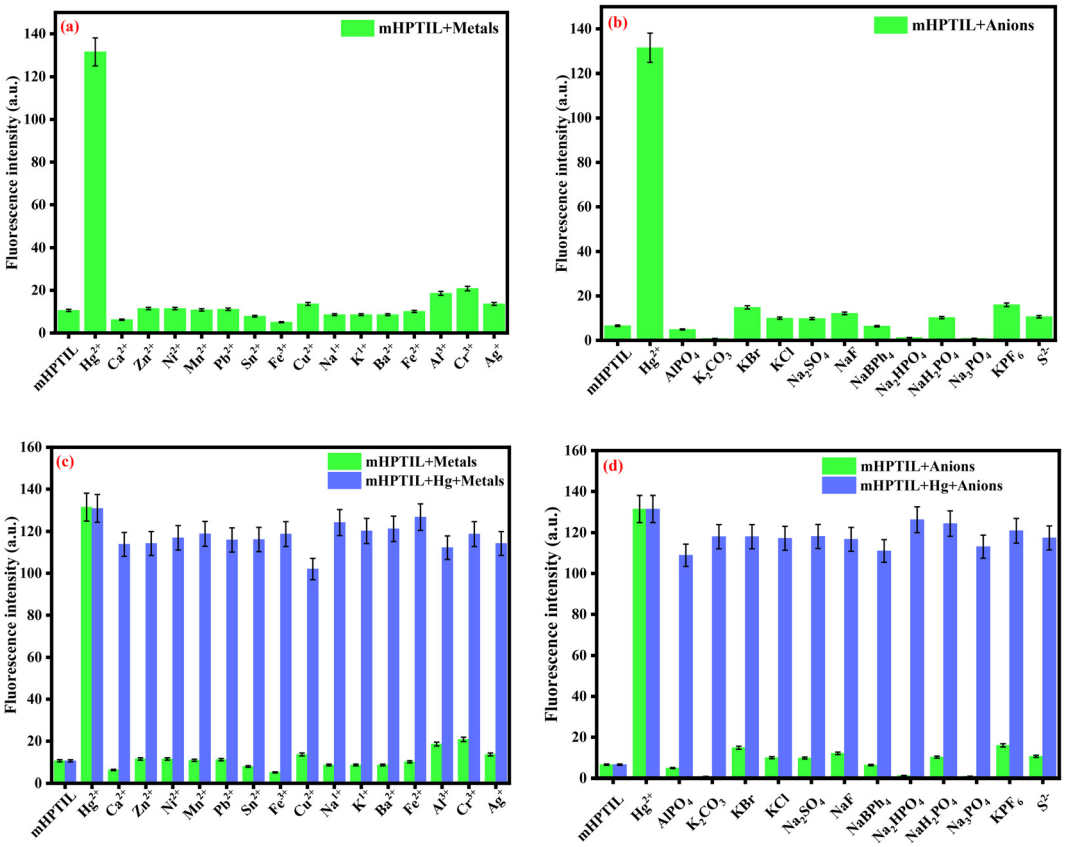

Fig. 6 Photoluminescence investigation of the interaction of **mHPTIL** (29 μM) at 426 nm, (a) upon introduction of various metal ions (96 μM) at 426 nm, (b) upon introduction of various anions (96 μM) at 426 nm, (c) with Hg^{2+} (96 μM) upon the interaction of other competing metal ions (96 μM) at 426 nm, and (d) with Hg^{2+} upon the interaction of other competing anions (96 μM) at 426 nm.

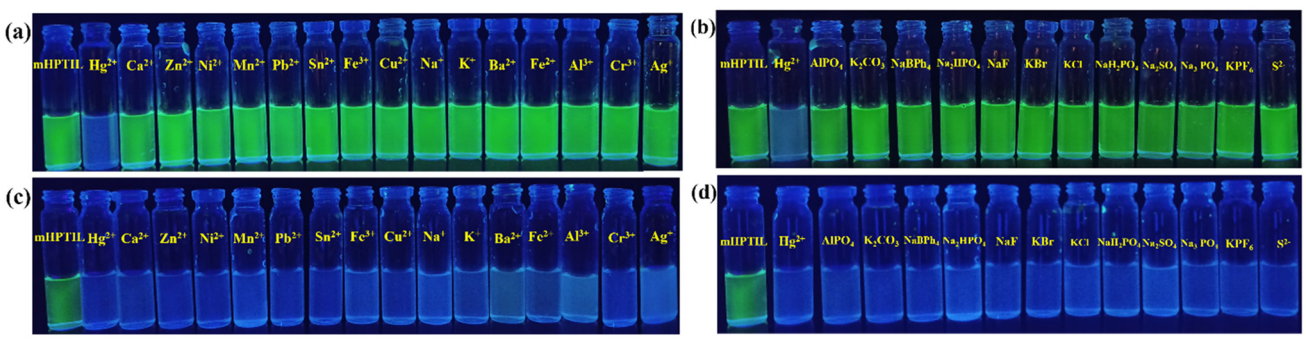

Fig. 7 Variation in the photoluminescence intensity of **mHPTIL** (29 μM) under 365 nm UV lamp irradiation towards the (a) selectivity of various metal ions (96 μM), (b) selectivity of various anions (96 μM), (c) interference of Hg^{2+} (96 μM) with the addition of different equally potent metal ions (96 μM), and (d) interference of Hg^{2+} (96 μM) with the addition of various equally potent anions (96 μM).

Therefore, we can conclude that pH 7.22 is well-suitable for the formation of the **mHPTIL**-Hg^{2+} complex. Based on these findings, it can be concluded that the **mHPTIL** optode is highly effective for detecting Hg^{2+} at a physiological pH.

Fabrication of paper-based test kits

Paper-based test strips are broadly used in analysis given their low cost, portability, speed, ease of use, and disposability.[77–79] Numerous detection methods, such as electrochemical analysis,[80,81] electrochemiluminescence,[80] chemiluminescence,[82] fluorescence,[83,84] and colorimetry,[85] can be incorporated into paper substrates. In this regard, a portable, low-cost photonic device using chemosensor-filled paper strips has gained admiration for the rapid on-site detection of various analytes. To validate real-world use, we established a paper strip test kit by dipping filter paper in aqueous **mHPTIL**, followed by

air drying. The strips show green fluorescence under 365 nm UV light. Metal ion detection was carried out using **mHPTIL**-based test strips. After applying various metal ions and drying, a distinct green-to-blue fluorescence shift under 365 nm UV light was observed, specifically with Hg^{2+}. The test kit shows high selectivity for Hg^{2+}, as other metal ions caused no significant fluorescence change under the same conditions (Fig. 8a), indicating successful on-site Hg^{2+} detection. Further, we quantified Hg^{2+} using **mHPTIL**-coated paper across 10^{-3} to 10^{-9} M. A consistent green-to-blue fluorescence shift confirmed its high sensitivity, highlighting its potential for portable, on-site photonic detection (Fig. 8b). In the field, such devices could be adapted for practical use, allowing for quick and easy visual detection and quantification of hazardous heavy metal, Hg^{2+}. Additionally, we used pure (neat) **HPTIL** on Whatman paper, and a cyan-to-blue fluorescence shift (447/488 nm to 438 nm) was observed upon adding Hg^{2+} (10^{-3} M), confirming its solvent-free detection capability and potential for environmental monitoring (Fig. 8c, CIE analysis, Fig. 8d). The color coordinate values (X = 0.142 and Y = 0.128), which lie under the color gamut of cyanish fluorescence, change to (X = 0.154 and Y = 0.0646), belonging to the blue color florescence after treatment with 2–3 drops of 10^{-3} M Hg^{2+} ions.

Real sample analysis

The sensor's high sensitivity to Hg^{2+} ions encouraged us to explore the potential real-world applications of **mHPTIL**, especially for heavy metal ion detection in the soil and water samples, as industrial wastewater is often contaminated with several heavy metal ions and many toxic elements pollute our environmental soil and water. To carry out this study, 0.5 g of soil was placed in a glass vial and spiked with 22 μL of Hg^{2+} ions at a concentration of 1×10^{-2} mol L^{-1}. The treated soil was then added to 2 mL of water-suspended solution and allowed to settle with a final concentration of 96 μM Hg^{2+} ions. Upon exposure to 365 nm UV light, a shift of fluorescence color from green to blue was observed, as demonstrated in (Fig. 9a). Further, fluorometric investigation was performed, which suggested a recovery percentage of more than 90% in the case of sand and field soil and 80% in the case of clay soil (Fig. 9b).

Given that water is the most abundant and vital liquid in biological systems, we extended our study to detect Hg^{2+} ions

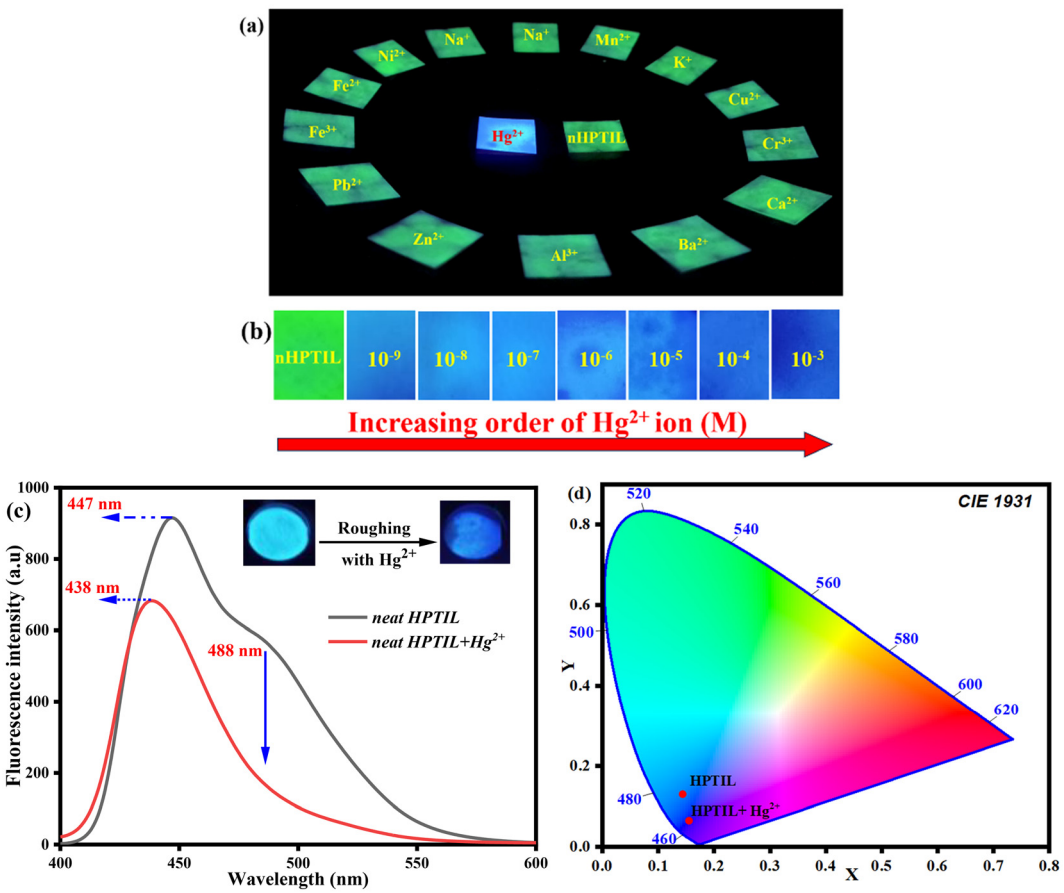

Fig. 8 (a) Optical validation for the selective detection of Hg^{2+} ions (few drops of 10^{-3} M) based on a solid-state paper-strip-based test kit and (b) addition of varying concentrations of Hg^{2+} ions (few drops from 10^{-3} M to 10^{-9} M) in the **mHPTIL**-coated filter paper, irradiated under a UV lamp of 365 nm. (c) Deviations in the photoluminescence spectra of neat **HPTIL**-packed filter paper with the addition of Hg^{2+} ions (a few drops of 10^{-3} M), λ_{exc} = 330 nm. (d) CIE illustration with the fluorogenic change in color gamut from cyan to blue for neat **HPTIL**-packed filter paper from X = 0.142 and Y = 0.128 to X = 0.154 and Y = 0.0646.

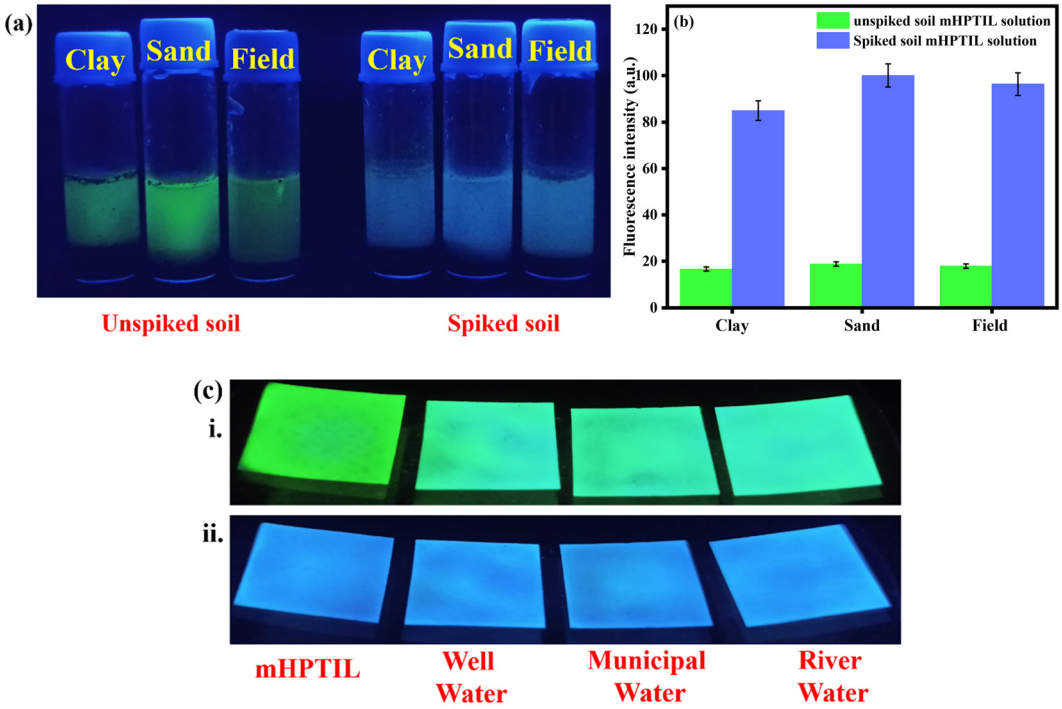

Fig. 9 (a) Validation of Hg^{2+} detection using unspiked and spiked **mHPTIL** solutions (spiked with 22 μL of Hg^{2+} ion) in different soils irradiated under a 365 nm UV lamp. (b) Bar plot demonstrating the change in photoluminosity of unspiked and spiked **mHPTIL** solutions in different soils at an emission wavelength of 426 nm. (c) Illustration of **mHPTIL**-coated paper strip test kit for environmental water sample, demonstrating the change in photoluminosity: (i) photoluminosity of **mHPTIL**-coated paper strip with different environmental water samples and (ii) photoluminosity after treatment of different environmental water samples spiked with Hg^{2+} ions (few drops of 10^{-3} M) on the **mHPTIL**-coated paper strip.

in real environmental water samples collected from Siliguri, West Bengal, India. These included municipal water, river water (Mahananda), and well water, which is mostly utilized as a source of drinking water within this locality. Alternatively, filter papers coated with **mHPTIL** and air-dried were used as test strips and were treated dropwise with the different Hg^{2}-spiked water samples. Remarkably, all treated strips exhibited a distinct fluorometric color change from green to blue under 365 nm UV light, as shown in Fig. 9c, suggesting that the optode has strong potential for environmental monitoring applications. Additionally, to quantify the environmental water sample, we examined the potency of our **mHPTIL** solution with river water (Mahananda, Siliguri) and well water (Siliguri). In each 2 mL volume of the sample, varying concentrations of Hg^{2+} were added, and the photoluminescence intensity was measured. The concentration is estimated by photoluminescence titration. Surprisingly, the recovery percentage of our sample towards the spiked river is more than 90%, while in the case of well water, the recovery is more than 85% (Table 1).

Our investigation into the sensor's performance for biomedical and forensic applications included testing its performance in biological fluids, specifically urine samples. We recorded the photoluminescence intensity of neat urine, urine combined with **mHPTIL**, and urine combined with **mHPTIL** and Hg^{2+} ion (Fig. S9†). These data lend credence to the conclusion that the **mHPTIL** optode is functional in biological fluids. In general, these practical findings highlight the effectiveness of **mHPTIL** in detecting Hg^{2+} ions across both environmental and biological matrices.

Table 1 Determination of Hg^{2+} in different water samples

Sample	Added (μM)	Found (μM)	Recovery (%)
River water	2.42	2.25	93.19
	4.83	4.47	92.67
	7.22	6.69	92.65
	9.61	8.66	90.10
	11.99	11.21	93.56
	14.35	13.34	93.00
	19.04	17.19	90.28
Well water	2.42	2.21	91.28
	4.83	4.12	85.39
	7.22	6.36	87.97
	9.61	8.25	85.82
	11.99	10.79	90.01
	14.35	12.93	90.13
	19.04	17.17	90.17

IL-based microparticle (mHPTIL) superiority against HPTS

Compared to standard materials, the cooperation of tunable materials with ionic liquids is of greater advantage. To assess its sensing competencies, we evaluated the performance of HPTS compared with IL-based low-dimensional materials (**mHPTIL**). This contrast was achieved by analyzing the detection of heavy metal Hg^{2+} utilizing both spectrophotometric

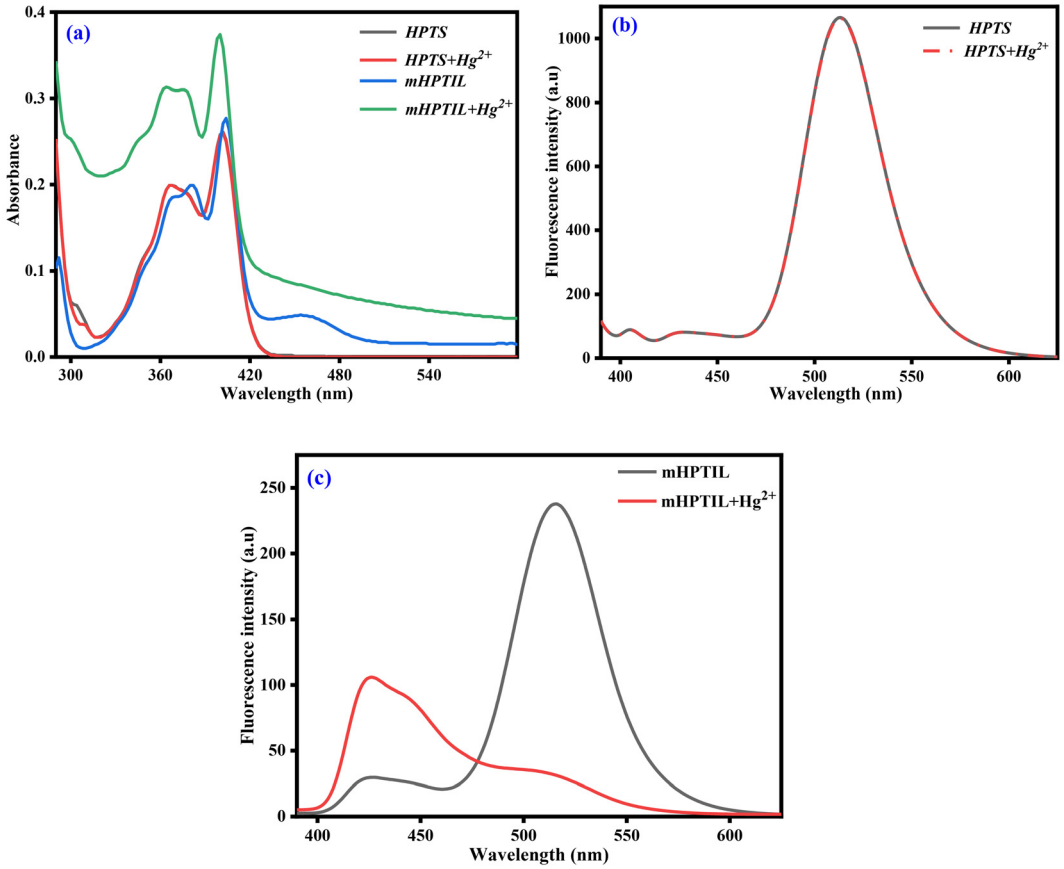

Fig. 10 (a) UV-visible absorption spectra of HPTS (2.49 μM), HPTS with the addition of Hg^{2+} (98 μM), **mHPTIL** (29 μM), and **mHPTIL** with the addition of Hg^{2+} (96 mM). (b) Photoluminescence peak of HPTS (2.49 μM) and HPTS with the addition of Hg^{2+} (98 μM), λ_{exc} = 330 nm. (c) Photoluminescence peak of **mHPTIL** (29 μM) and **mHPTIL** with the addition of Hg^{2+} (96 μM), λ_{exc} = 330 nm.

and fluorometric methods for HPTS and **mHPTIL**. The addition of Hg^{2+} to HPTS in the aqueous solution did not alter the absorption spectra according to UV-visible spectrophotometric experiments (Fig. 10a). The photoluminescence intensity of HPTS in aqueous solution persisted virtually unaffected upon the addition of Hg^{2+} (Fig. 10b), indicating that HPTS is ineffective for Hg^{2+} detection. In contrast, introducing Hg^{2+} to the **mHPTIL** solution led to a noticeable blue shift of 4 nm in the absorption spectrum, accompanied by an increase in Mie scattering (Fig. 10a). Additionally, we detected a shift in the emission peak from 515 to 426 nm in the photoluminescence experiments, along with a noticeable fluorometric change from greenish to bluish when exposed to 365 nm UV light irradiation, demonstrating its effectiveness in the detection of Hg^{2+} (Fig. 10c). In the construction of IL-based heavy metal Hg^{2+}-sensitive low-dimensional materials, the ultra-hydrophobic cationic constituent of **HPTIL** establishes three crucial roles. First, it contributes to the fruitful materialization of the IL structure. Second, it establishes robust hydrophobic interactions with the signaling unit, $[HPTS]^{3-}$, anchoring it firmly onto the filter paper. This interaction effectively prevents the leaching of $[HPTS]^{3-}$ signaling moieties into the experimental solution. Third, the material reacts quickly in the presence of Hg^{2+} because of its extremely hydrophobic characteristics, showing repulsive behavior towards water molecules, which fastens the drying process. Therefore, we may conclude that low-dimensional materials based on synthesized ILs, or **mHPTIL**, are superior to conventional ones.

Conclusion

An Hg^{2+} ion responsive IL, **HPTIL**, and its microparticle **mHPTIL** are introduced based on hydroxyproline-1,3,6-trisulfonate as a signalling moiety. In contrast to non-ILs, **HPTIL** produces microparticles in aqueous environments that have several significant photophysical characteristics. The microoptode exhibits a remarkable ability to detect Hg^{2+} ions, displaying a visible fluorogenic shift from green to blue under a UV lamp of 365 nm wavelength. It achieves detecting limits and quantifying limits under the nanomolar (nM) range, outperforming many previously reported sensors (Table S1†). The practical utility of our optode was established through the investigation of water and soil samples, opening avenues for broader applications across various fields. Additionally, we appraised the optode's aptitude to detect Hg^{2+} ions using cost-

effective test strips. Further investigation reveals that both neat **HPTIL** and water-suspended **mHPTIL** are very efficient for detecting Hg^{2+} ions. The present report advocates a new technique for developing sophisticated functional optoelectronic materials by integrating the advantageous physicochemical characteristics of ILs into their fundamental structures. The current report also demonstrates IL-based nanoparticles with controlled aggregation behavior for bright, stable signaling, enabling precise analysis of various target analytes, which is of paramount importance to the scientific communities for the development of next-generation sensing devices.

Conflicts of interest

There is no conflicts of interest to declare.

Data availability

The data supporting this article have been included as part of the ESI.†

Acknowledgements

Thanks to Anusandhan National Research Foundation (ANRF), former Science and Engineering Research Board (SERB), New Delhi, Govt of India, (File No: EEQ/2023/000048) for the funding. SA thanks ANRF for the fellowship awarded to him. NT is indebted to the Ministry of Minority Affairs for the *Maulana Azad National Fellowship* awarded to her.

References

1 F. Di Natale, A. Lancia, A. Molino, M. Di Natale, D. Karatza and D. Musmarra, *J. Hazard. Mater.*, 2006, **132**, 220–225.
2 U. Förstner and G. T. W. Wittmann, *Met. Pollut. Aquat. Environ.*, 1981, DOI: 10.1007/978-3-642-69385-4.
3 L. T. Budnik and L. Casteleyn, *Sci. Total Environ.*, 2019, **654**, 720–734.
4 C. Zamora-Ledezma, D. Negrete-Bolagay, F. Figueroa, E. Zamora-Ledezma, M. Ni, F. Alexis and V. H. Guerrero, *Environ. Technol. Innovation*, 2021, **22**, 101504.
5 N. A. A. Qasem, R. H. Mohammed and D. U. Lawal, *npj Clean Water*, 2021, **4**, 1–15.
6 K. H. Vardhan, P. S. Kumar and R. C. Panda, *J. Mol. Liq.*, 2019, **290**, 111197.
7 J. P. Vareda, A. J. M. Valente and L. Durães, *J. Environ. Manage.*, 2019, **246**, 101–118.
8 J. S. Crosby, D. Lucas and C. P. Koshland, *Sens. Actuators, B*, 2013, **181**, 938–942.
9 V. L. Cariccio, A. Samà, P. Bramanti and E. Mazzon, *Biol. Trace Elem. Res.*, 2018, **187**, 341–356.
10 H. H. Harris, I. J. Pickering and G. N. George, *Science*, 2003, **301**, 1203.
11 Q. Wang, D. Kim, D. D. Dionysiou, G. A. Sorial and D. Timberlake, *Environ. Pollut.*, 2004, **131**, 323–336.
12 L. Zhao, Z. Zhang, Y. Liu, J. Wei, Q. Liu, P. Ran and X. Li, *J. Hazard. Mater.*, 2020, **385**, 121556.
13 H. Na Kim, W. Xiu Ren, J. Seung Kim and J. Yoon, *Chem. Soc. Rev.*, 2012, **41**, 3210–3244.
14 M. M. Pires and J. Chmielewski, *Org. Lett.*, 2008, **10**, 837–840.
15 K. P. Lisha, Anshup and T. Pradeep, *Gold Bull.*, 2009, **42**, 144–152.
16 N. E. Selin, *Annu. Rev. Environ. Resour.*, 2009, **34**, 43–63.
17 L. Y. Kurland, S. N. Faro and H. Siedler, Minamata Disease The Outbreak of a Neurologic Disorder in Minamata, Japan, and Its Relationship to the Ingestion of Seafood Contaminated by Mercurial Compounds, *World Neurol.*, 1960, **1**, 370–375; . - References - Scientific Research Publishing, https://www.scirp.org/reference/ReferencesPapers?ReferenceID=2314318, (accessed 27 April 2025).
18 T. W. Clarkson, L. Magos and G. J. Myers, *N. Engl. J. Med.*, 2003, **349**, 1731–1737.
19 A. K. Mahapatra, G. Hazra, N. K. Das, P. Sahoo, S. Goswami and H. K. Fun, *J. Photochem. Photobiol., A*, 2011, **222**, 47–51.
20 J. S. Zhu, *Inorganic chemistry*, Science Press, Beijing, 2008, p. 393. Search Videos, https://www.bing.com/videos/search?q=ZhuJS(2008)+Inorganic+chemistry.+Science+Press%2C+Beijing%2C+p+393&qpvt=ZhuJS(2008)+Inorganic+chemistry.+Science+Press%2C+Beijing%2C+p+393&FORM=VDRE, (accessed 27 April 2025).
21 X. Zhu, L. Chen, Z. Lin, B. Qiu and G. Chen, *Chem. Commun.*, 2010, **46**, 3149–3151.
22 S. J. Liu, H. G. Nie, J. H. Jiang, G. L. Shen and R. Q. Yu, *Anal. Chem.*, 2009, **81**, 5724–5730.
23 I. Narin, M. Soylak, L. Elçi and M. Doğan, *Talanta*, 2000, **52**, 1041–1046.
24 E. Witkowska, K. Szczepaniak and M. Biziuk, *J. Radioanal. Nucl. Chem.*, 2005, **265**, 141–150.
25 B. Sun, X. Jiang, H. Wang, B. Song, Y. Zhu, H. Wang, Y. Su and Y. He, *Anal. Chem.*, 2015, **87**, 1250–1256.
26 Y. Zhu, X. Jiang, H. Wang, S. Wang, H. Wang, B. Sun, Y. Su and Y. He, *Anal. Chem.*, 2015, **87**, 6631–6638.
27 P. Ugo, L. M. Moretto, P. Bertoncello and J. Wang, *Electroanalysis*, 1998, **10**, 1017–1021.
28 A. Shafawi, L. Ebdon, M. Foulkes, P. Stockwell and W. Corns, *Analyst*, 1999, **124**, 185–189.
29 N. Tohora, R. Sahoo, S. Ahamed, J. Chourasia, S. Lama, M. Mahato, S. Ali and S. K. Das, *Phys. Chem. Chem. Phys.*, 2025, **27**, 9478–9490.
30 T. Sultana, M. Mahato, S. Ahamed, N. Tohora, J. Chourasia, S. Ghanta and S. Kumar Das, *J. Photochem. Photobiol., A*, 2025, **459**, 116028.
31 R. Ali, I. A. I. Ali, S. Messaoudi, F. M. Alminderej and S. M. Saleh, *J. Mol. Liq.*, 2021, **336**, 116122.
32 J. Hu, X. Yu, X. Zhang, C. Jing, T. Liu, X. Hu, S. Lu, K. Uvdal, H. W. Gao and Z. Hu, *Spectrochim. Acta, Part A*, 2020, **241**, 118657.

33 S. Xue, P. Wang and K. Chen, *Spectrochim. Acta, Part A*, 2020, **226**, 117616.
34 R. D. Rogers, K. R. Seddon and S. Volkov, ed., *Ionic Liquids - Solvents of the Future?*, 2003, DOI: **10.1007/978-94-010-0127-4**.
35 T. Welton, *Chem. Rev.*, 1999, **99**, 2071–2083.
36 N. V. Plechkova and K. R. Seddon, *Chem. Soc. Rev.*, 2007, **37**, 123–150.
37 T. Welton, *Biophys. Rev.*, 2018, **10**, 691–706.
38 J. S. Wilkes, *Green Chem.*, 2002, **4**, 73–80.
39 Green Sustainable Process for Chemical and Environmental Engineering and Science | ScienceDirect, **https://www.sciencedirect.com/book/9780323851466/green-sustainable-process-for-chemical-and-environmental-engineering-and-science#book-info**, (accessed 27 April 2025).
40 J. D. Scholten, B. C. Leal and J. Dupont, *ACS Catal.*, 2012, **2**, 184–200.
41 K. Matsumoto, J. Hwang, S. Kaushik, C. Y. Chen and R. Hagiwara, *Energy Environ. Sci.*, 2019, **12**, 3247–3287.
42 R. A. Perera Jayawickramage and J. P. Ferraris, *Nanotechnology*, 2019, **30**, 155402.
43 D. Blanco, R. González, J. L. Viesca, A. Fernández-González, M. Bartolomé and A. Hernández Battez, *Tribol. Lett.*, 2017, **65**, 1–10.
44 H. Xiao, *Tribol. Trans.*, 2017, **60**, 20–30.
45 M. Mahato, Y. Murakami and S. K. Das, *Appl. Mater. Today*, 2023, **32**, 101808.
46 M. E. V. Valkenburg, R. L. Vaughn, M. Williams and J. S. Wilkes, *Thermochim. Acta*, 2005, **425**, 181–188.
47 F. Billeci, H. Q. Nimal Gunaratne, F. D'anna, G. G. Morgan, K. R. Seddon and N. V. Plechkova, *Green Chem.*, 2019, **21**, 1412–1416.
48 C. Rizzo, S. Marullo, N. T. Dintcheva and F. D'Anna, *Molecules*, 2019, **24**, 2788.
49 C. Rizzo, J. L. Andrews, J. W. Steed and F. D'Anna, *J. Colloid Interface Sci.*, 2019, **548**, 184–196.
50 F. Billeci, F. D'Anna, H. Q. N. Gunaratne, N. V. Plechkova and K. R. Seddon, *Green Chem.*, 2018, **20**, 4260–4276.
51 C. Rizzo, S. Marullo, N. T. Dintcheva, C. Gambarotti, F. Billeci and F. D'Anna, *J. Colloid Interface Sci.*, 2019, **556**, 628–639.
52 P. C. Marr and A. C. Marr, *Green Chem.*, 2015, **18**, 105–128.
53 C. Rizzo, F. D'Anna and R. Noto, *RSC Adv.*, 2016, **6**, 58477–58484.
54 J. Zhao, Y. Yue, G. Sheng, B. Wang, H. Lai, S. Di, Y. Zhai, L. Guo and X. Li, *Chem. Eng. J.*, 2019, **360**, 38–46.
55 R. L. Vekariya, *J. Mol. Liq.*, 2017, **227**, 44–60.
56 T. Itoh, *Chem. Rev.*, 2017, **117**, 10567–10607.
57 W. I. S. Galpothdeniya, F. R. Fronczek, M. Cong, N. Bhattarai, N. Siraj and I. M. Warner, *J. Mater. Chem. B*, 2016, **4**, 1414–1422.
58 I. M. Warner, B. El-Zahab and N. Siraj, *Anal. Chem.*, 2014, **86**, 7184–7191.
59 P. K. S. Magut, S. Das, V. E. Fernand, J. Losso, K. McDonough, B. M. Naylor, S. Aggarwal and I. M. Warner, *J. Am. Chem. Soc.*, 2013, **135**, 15873–15879.
60 J. Z. Du, X. J. Du, C. Q. Mao and J. Wang, *J. Am. Chem. Soc.*, 2011, **133**, 17560–17563.
61 H. Kasai, T. Murakami, Y. Ikuta, Y. Koseki, K. Baba, H. Oikawa, H. Nakanishi, M. Okada, M. Shoji, M. Ueda, H. Imahori and M. Hashida, *Angew. Chem., Int. Ed.*, 2012, **51**, 10315–10318.
62 S. Che, A. Xu, Q. Shou, L. Yin, C. Zhou, H. Fu and Y. She, *Anal. Chim. Acta*, 2022, **1232**, 340396.
63 N. Tohora, S. Ahamed, T. Sultana, M. Mahato and S. K. Das, *Talanta*, 2024, **266**, 124968.
64 G. Sahay, J. O. Kim, A. V. Kabanov and T. K. Bronich, *Biomaterials*, 2010, **31**, 923–933.
65 S. Che, L. Yin, Y. Fan, Q. Shou, C. Zhou, H. Fu and Y. She, *Sens. Actuators, B*, 2022, **360**, 131588.
66 Y. B. Barot, V. Anand and R. Mishra, *J. Phys. Chem. B*, 2023, **127**, 10529–10541.
67 K. Y. Yung, A. J. S. Hewitt, N. P. Hunter, F. V. Bright and G. A. Baker, *Chem. Commun.*, 2011, **47**, 4775–4777.
68 K. Yamaguchi, S. Sakamoto, H. Tsuruta and T. Imamoto, *Chem. Commun.*, 1998, 2123–2124.
69 R. D. Pensack, R. J. Ashmore, A. L. Paoletta and G. D. Scholes, *J. Phys. Chem. C*, 2018, **122**, 21004–21017.
70 S. Das, P. K. S. Magut, S. L. De Rooy, F. Hasan and I. M. Warner, *RSC Adv.*, 2013, **3**, 21054–21061.
71 S. H. Kim, H. S. Choi, J. Kim, S. J. Lee, D. T. Quango and J. S. Kim, *Org. Lett.*, 2010, **12**, 560–563.
72 H. A. Benesi and J. H. Hildebrand, *J. Am. Chem. Soc.*, 1949, **71**, 2703–2707.
73 S. Che, L. Yin, Y. Fan, Q. Shou, C. Zhou, H. Fu and Y. She, *Sens. Actuators, B*, 2022, **360**, 131588.
74 Y. Y. Wang, X. Xiang, R. Yan, Y. Liu and F. L. Jiang, *J. Phys. Chem. C*, 2018, **122**, 1148–1157.
75 M. M. Yin, P. Dong, W. Q. Chen, S. P. Xu, L. Y. Yang, F. L. Jiang and Y. Liu, *Langmuir*, 2017, **33**, 5108–5116.
76 R. Yan, L. Lai, Z. Q. Xu, F. L. Jiang and Y. Liu, *Wuli Huaxue Xuebao*, 2017, **33**, 2377–2387.
77 J. C. Cunningham, P. R. Degregory and R. M. Crooks, *Annu. Rev. Anal. Chem.*, 2016, **9**, 183–202.
78 Z. Lin, S. Lv, K. Zhang and D. Tang, *J. Mater. Chem. B*, 2017, **5**, 826–833.
79 R. Liu, E. M. McConnell, J. Li and Y. Li, *J. Mater. Chem. B*, 2020, **8**, 3213–3230.
80 L. Ge, J. Yan, X. Song, M. Yan, S. Ge and J. Yu, *Biomaterials*, 2012, **33**, 1024–1031.
81 S. Y. Yeon, M. Seo, Y. Kim, H. Hong and T. D. Chung, *Biosens. Bioelectron.*, 2022, **203**, 114002.
82 J. L. Delaney, C. F. Hogan, J. Tian and W. Shen, *Anal. Chem.*, 2011, **83**, 1300–1306.
83 H. Zhang, Z. Zhao, Z. Lei and Z. Wang, *Anal. Chem.*, 2016, **88**, 11358–11363.
84 Z. Qiu, J. Shu and D. Tang, *Anal. Chem.*, 2017, **89**, 5152–5160.
85 K. F. Lei, C. H. Huang, R. L. Kuo, C. K. Chang, K. F. Chen, K. C. Tsao and N. M. Tsang, *Anal. Chim. Acta*, 2015, **883**, 37–44.